Electronic Supplementary Material (ESI) for Journal of Materials Chemistry A.
This journal is © The Royal Society of Chemistry 2018

Supporting Information

Oxygen redox in hexagonal layered Na_xTMO_3 (TM = 4d elements) for high capacity Na ion batteries

M. Hussein N. Assadi,[†,‡] Masashi Okubo, [§,⊥] Atsuo Yamada, [§,⊥] Yoshitaka Tateyama[*,†,⊥,‖]

[†]Center for Green Research on Energy and Environmental Materials (GREEN), National Institute for Materials Science (NIMS), 1-1 Namiki, Tsukuba, Ibaraki 305-0044, Japan.

[‡]Center for Computational Sciences, University of Tsukuba, Tennodai 1-1-1, Tsukuba, Ibaraki 305-8577, Japan.

[§]Department of Chemical System Engineering, The University of Tokyo, 7-3-1 Hongo, Bunkyo-ku, Tokyo 113-8656, Japan.

[⊥]Elements Strategy Initiative for Catalysts & Batteries (ESICB), Kyoto University, 1-30 Goryo-Ohara, Nishikyo-ku, Kyoto 615-8245, Japan.

[‖]Center for Materials Research by Information Integration (CMI2) & International Center for Materials Nanoarchitectonics (MANA), National Institute for Materials Science (NIMS), 1-1, Namiki, Tsukuba 305-0044, Japan.

KEY WORDS: *Na ion battery, Na cathode, O redox, O2 evolution*

1. ADDITIONAL COMPUTATIONAL SETTINGS

The pseudopotentials used in calculations contained the following electrons: $1s^2 2p^4$ for O; $2p^6 3s^1$ for Na, $4p^6 4d^4 5s^1$ for Nb, $4p^6 4d^5 5s^1$ for Mo; $4p^6 4d^5 5s^2$ for Tc; $4p^6 4d^7 5s^1$ for Ru; $4p^6 4d^8 5s^1$ for Rh; $4p^6 4d^{10}$ for Pd; and $4d^{10} 5s^1$ for Ag. The k-point mesh for Bouillon zone integration was always generated with ~0.02 $Å^{-1}$ spacing. That translated into a 17×17×9 Monkhorst-Pack mesh for the $R\bar{3}m$ hexagonal Na_1RuO_2 (shown in Figure S2), a 11×11×3 mesh for $R\bar{3}$ Na_1TMO_3 and a 11×11×9 mesh for $P\bar{3}1m$ $Na_{0.5}RuO_3$. All structures were fully relaxed until the all Cartesian components acting on the ions were smaller than 0.01 eV/Å. The formation energy (E^f) of the Na vacancies was calculated using the following standard formula:

$$E^f = E^t(\mathrm{Na}_x\mathrm{RuO}_3) - E^t(\mathrm{Na}_{x-1}\mathrm{RuO}_3) - \mu_{\mathrm{Na}}. \qquad \text{(Eq. S1).}$$

Here, $E^t(Na_xRuO_3)$ is the total energy of the original supercell without Na vacancy, $E^t(Na_{x-1}RuO_3)$ the total energy of the supercell containing one Na vacancy and μ_{Na} are the chemical potential of Na ions calculated from the total energy of Na metallic phases.

2. CHOICE OF FUNCTIONAL

We examined the dependence of the calculated electronic and structural properties of the $R\bar{3}$ Na_1RuO_3, using general gradient approximation (GGA), GGA+U and hybrid functionals (HSE03 implementation with a mixing parameter of 0.2). The total destiny and partial of states is presented in Figure S1, while the band gap, lattice parameters and O electronic population within -2 eV $< E < E_{Fermi}$ are presented in

Table S1. GGA method predicts a nonmagnetic metallic state which is incorrect. GGA+U method, even for U_{eff} = 1 eV, predicts the correct local magnetization of the Ru ions and results in a small bang gap. The value of the band gap increases with the increasing U_{eff}. However, for U_{eff} = 2 eV, the GGA+U results are very similar to those of hybrid method. That is also true for the O population near the Fermi level which is sensitive to the choice of functional. Furthermore, we examined the electronic structure of the fully desodiated $Na_{0.5}RuO_3$ compound calculated with both GGA+U with U_{eff} = 2 eV and hybrid HSE03 functionals. Both functional also produced similar density of states and O electronic population near the Fermi level. GGA+U method resulted in 0.920 e/O for -2 eV < E < E_{Fermi} while HSE03 functional resulted in a population of 0.973 e/O for the same energy range. Since the results with GGA+U functional (U_{eff} = 2 eV) are comparable to those of HSE03, we chose the GGA+U for the calculations presented in this work as they are computationally less demanding.

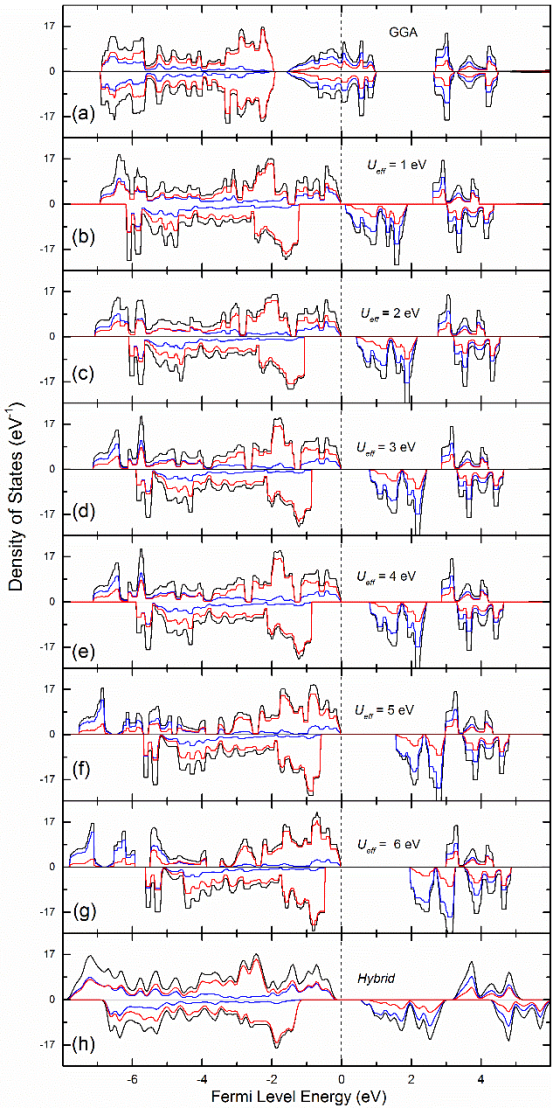

Figure S1. Total and partial density of states of $R\bar{3}$ Na_1RuO_3 calculated with different functionals. The black, red and blue lines represent the total, O 2p states and Ru 4d states respectively. Energy is represented with respect to the Fermi level.

Table S1. The structural and electronic characteristics of $R\bar{3}$ Na_1RuO_3 calculated with GGA, GGA+U and hybrid functional.

Functional	Band gap (eV)	*a* (Å)	*c* (Å)	Conduction	O population (e/O)
GGA	–	5.345	15.481	Metallic	0.282
GGA+U (U_{eff} = 1)	0.12	5.248	15.521	Insulator	1.157
GGA+U (U_{eff} = 2)	0.45	5.242	15.559	Insulator	1.429
GGA+U (U_{eff} = 3)	0.84	5.245	16.080	Insulator	1.749
GGA+U (U_{eff} = 4)	1.19	5.250	16.074	Insulator	1.949
GGA+U (U_{eff} = 5)	1.59	5.254	16.082	Insulator	2.044
GGA+U (U_{eff} = 6)	1.99	5.248	16.100	Insulator	2.166
HSE03	0.52	5.241	15.560	Insulator	1.382

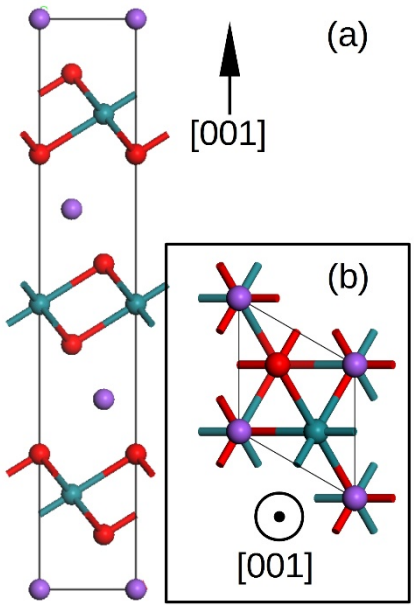

Figure S2. The O3 $R\bar{3}m$ Na_1RuO_2 cell that was used to construct Na_2RuO_3 structure. The calculated lattice parameters were 3.14 Å and 15.93 Å for *a* and *c* respectively. The green, purple and red spheres represent Ru, Na and O ions respectively.

3. SODIATED AND DESODIATED Na_2RuO_3

In order to obtain the structure model for $R\bar{3}m$ Na_2RuO_3, we constructed a $\sqrt{3}a\times\sqrt{3}a\times1$ supercell of O3 $NaRuO_2$ (shown in Figure S2) which resulted in a supercell with $Na_9Ru_9O_{18}$ formula. We then replaced 3 Ru ions with Na ions in a fashion that preserved the hexagonal symmetry of the system. The desodiated $R\bar{3}m$ structures were created by removing three Na ions and six Na ions in order to construct the $Na_{1.5}RuO_3$ and Na_1RuO_3 supercells respectively.

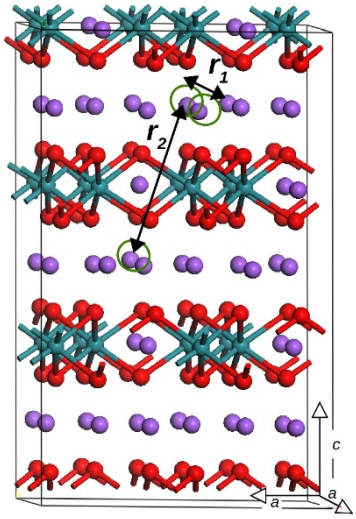

Figure S3. A schematic representation of the $Na_{46}Ru_{24}O_{72}$ or $Na_{1.84}RuO_3$ supercell containing two Na vacancies for which the sites of Na extraction are marked by circles. The green, purple and red spheres represent Ru, Na and O ions respectively.

To determine how V_{Na}s are spatially distributed during the early desodiation process, we calculated the total energy of a supercell containing two Na vacancies as shown in Figure S3. We chose two such configurations

that represent the extreme scenarios: (a) compact configuration in which the Na vacancies were created by removing two nearest neighbour Na ions with a separation of r_1 = 3.21 Å and (b) a disperse configuration in which the extracted Na ions were located at the furthest permissible distance of r_2 = 7.24 Å. The disperse configuration was found to be more stable by 25 meV indicating the preference of V_{Na}s to be dispersedly distributed.

Figure S4 shows the spin density of $R\bar{3}m$ Na_xRuO_3 for x = 2, 1.5 and 1. The non-zero spin density on O ions indicate the localization of the holes that are created by Na extraction on O ion. As a result, O's spin density infers O's participation in the redox reaction.

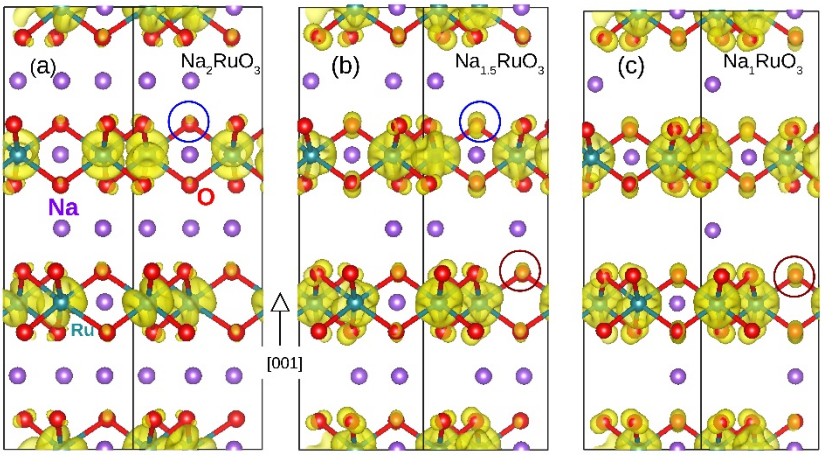

Figure S4. Spin isosurface drawn at density pf 0.03 e/A^3 for Na_2RuO_3, $Na_{1.5}RuO_3$ and Na_1RuO_3 in presented in (a), (b) and (c) respectively. The blue and brown circles show the progressive oxidization of O ions upon Na extraction.

4. STABILITY OF Na_1TMO_3 (TM = 4d) PHASE

We calculated the formation enthalpy of the $R\bar{3}$ Na_1TMO_3 against metallic Na and TM phases and O_2 gas using the following formula:

$$\Delta H_{metallic} = E^{total}(\mathrm{Na_1TMO_3}) - E^{total}(\mathrm{Na}) - E^{total}(\mathrm{TM}) - \frac{3}{2}E^{total}(\mathrm{O_2}) \qquad \text{(Eq. S2)}$$

in which the $E^{total}(Na_1TMO_3)$ is the total energy of $R\bar{3}$ Na_1TMO_3 compound, E^{total}(Na) and E^{total}(TM) are the total energy of the metallic phase Na and TM elements. $E^{total}(O_2)$ is the total energy of O_2 molecule. $\Delta H_{metallic}$ corresponds to the stability in O poor environment. The results are presented in Table S2. All compounds exhibit a negative $\Delta H_{metallic}$ indicating the stability against metallic species. Noticeably, $\Delta H_{metallic}$ has an inverse relationship with the atomic number of the TM ions indicating greater stability for compounds with earlier 4d TM elements.

We also examined the stability of $R\bar{3}$ Na_1TMO_3 with respect to the competing Na_2O and common TM oxide phases by calculating the formation enthalpy (ΔH_{oxide}) with respect to each TM's most stable oxide. ΔH_{oxide} corresponds to the stability in O rich environment. As shown in the third and fourth column of Table S2, except for Na_1AgO_3, all $R\bar{3}$ Na_1TMO_3 compounds were stable with respect to the competing oxide phases.

This implies that Na_1AgO_3 has to be synthesised using non-equilibrium methods in order to avoid the formation of competing oxide phases.

Magnetically, we examined the energy difference between ferromagnetic (FM) and antiferromagnetic (AFM) spin coupling in Na_1Mo_3, Na_1TcO_3, Na_1RuO_3, Na_1RhO_3 and Na_1PdO_3. Except for Na_1TcO_3, in all other compounds, the difference between E_{AFM}^{total} and E_{FM}^{total} was in the range of few meVs indicating lack of long range magnetic coupling at room temperature. E_{FM}^{total} in Na_1TcO_3 was more stable by 0.38 eV indicating possible room temperature ferromagnetic ordering. These features exhibit rather delocalized (less correlated) natures of 4d transition metal oxide systems.

Table S2. Phase stability of $R\bar{3}$ Na_1TMO_3.

compound	$\Delta H_{metallic}$ (eV/u.f.)	Competing oxide phases	ΔH_{oxide} (eV/u.f.)
Na_1NbO_3	−11.090	NbO, Na_2O, O_2	−7.025
Na_1MoO_3	−8.228	MoO_2, Na_2O,O_2	−2.152
Na_1TcO_3	−6.488	TcO_2, Na_2O, O_2	−1.902
Na_1RuO_3	−5.108	RuO_2, Na_2O,O_2	−1.549
Na_1RhO_3	−3.647	Rh_2O_3,Na_2O,O_2	−1.269
Na_1PdO_3	−2.479	PdO,Na_2O,O_2	−0.862
Na_1AgO_3	−0.839	Ag_2O,Na_2O,O_2	0.547

5. O REDOX IN Na_1NbO_3 AND Na_1AgO_3

Figure S5 and Figure S6 show the density of states of Na_xNbO_3 and Na_xAgO_3 in $R\bar{3}$ (x = 1) and desodiated $P\bar{3}1m$ (x = 0.5) phases respectively. In both compounds, desodiation to x = 0.5 results in O reduction as evidenced by the O 2p states near the Fermi level in both compounds. In both $Na_{0.5}NbO_3$ and $Na_{0.5}AgO_3$, O ions had a magnetization of ~0.16 e while the magnetization of the Nb and Ag remained zero as in Na_1NbO_3 and Na_1AgO_3 indicating the creation of a delocalised hole on O ions upon the extraction of Na ions. The average voltage between x = 1 and x = 0.5 for Na_1NbO_3 and Na_1AgO_3 was found to be 4.91 V and 4.30 V respectively.

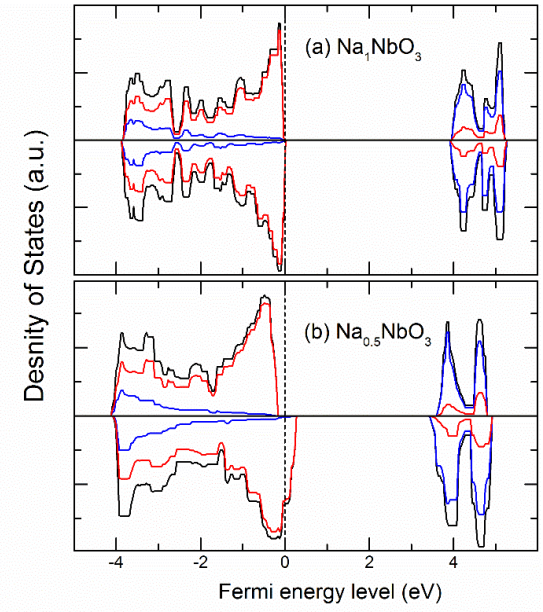

Figure S5. Total and partial destiny of states of (a) $R\bar{3}$ Na_1NbO_3 and (b) $P\bar{3}1m$ $Na_{0.5}NbO_3$. Black and red and blue lines represent total and O 2p states and Nb 4d states respectively.

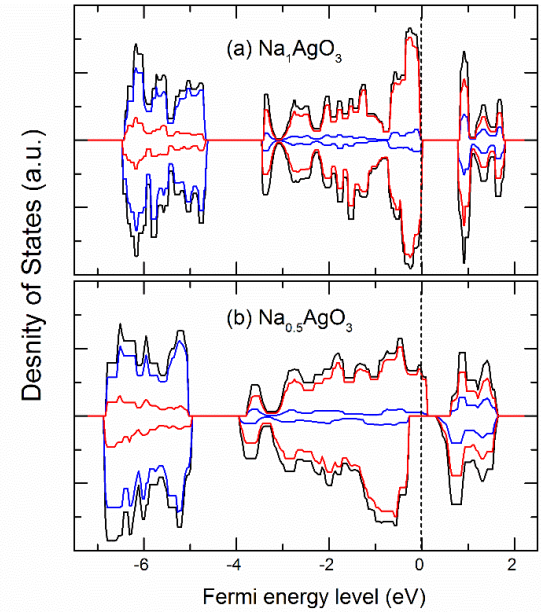

Figure S6. Total and partial destiny of states of (a) $R\bar{3}$ Na_1AgO_3 and (b) $P\bar{3}1m$ $Na_{0.5}AgO_3$. Black and red and blue lines represent total and O 2p states and Ag 4d states respectively.

6. LACK OF SIGMA BONDING AMONG O IONS IN $R\bar{3}$ COMPOUNDS

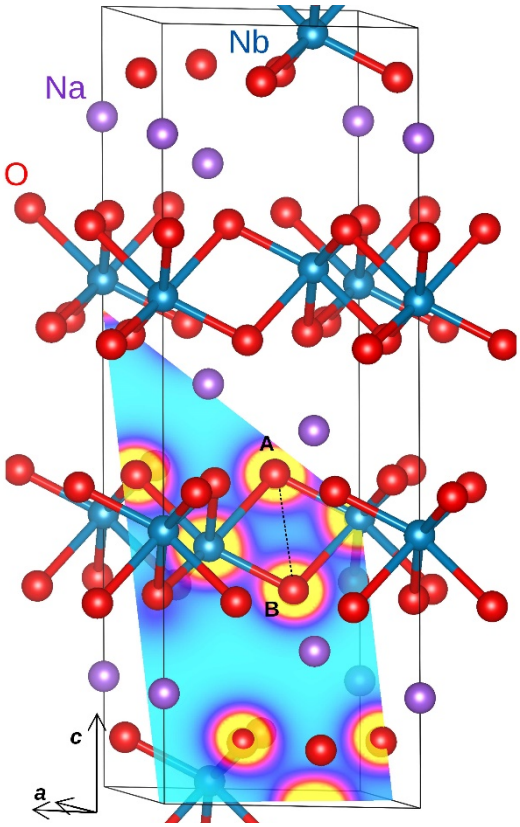

Figure S7. Cross-sectional charge density in Na_1NbO_3. The slice crosses two neighbouring oxygen ions. The miller index for the slice is (−1.0000, 2.6667, −4.0000). Yellow and Cyan fields correspond to maximum and zero charge density respectively.

Due the shorter distance among O ions in ilmenite type phase, one may anticipate sigma bond formation between O ions which in turn would lead to higher redox activity beyond that of a single electron of the TM ion. Hypothetically, the antibonding electron of this bond would make a great contribution to the density of states near the Fermi level. One requirement for the formation of sigma bond is having eligible orientation between O ions that allows the head to head overlap of the free orbitals. As predicted by our simulation, Na_1NbO_3 has the highest voltage and capacity. Its structure is presented in Figure S7. The smallest distance between any two oxygen ions (points A and B) is 2.58 Å. These O ions each themselves are also bound to two Nb ions. Since these two oxygen ions and their closest Nb ion are located to a good approximation in one plane, the formation of an additional sigma bond among these O ions is impossible. The vanishing charge density in the middle of the line connecting these two oxygen ions (AB in Figure S7) further proves the absence of sigma bonding. The examination of the charge density and the distance between O ions in the other $R\bar{3}$ compounds yielded the same result. More particularly, in none of the compounds the distance between closest O ions was shorter than 2.5 Å.